Structural health monitoring meets data mining

Miao, S.

Chapter 7

Modal Analysis

7.1 Background

In the Structural Health Monitoring field, damage detection methods are based on the premise that global modal parameters (natural frequencies, mode shapes and damping ratios) are functions of physical properties (mass, damping distribution, and stiffness) [45, 49, 112]. Changes in physical properties will cause changes in the modal parameters [40, 43, 49].

Modal analysis is a procedure that extracts modal parameters of a structure from its measured response data. Modal analysis was originally used for Experimental Modal Analysis (EMA), primarily applied to aerospace and mechanical structures, where the structures are excited by controlled dynamic forces. The responses to these forces are then recorded, and the modal parameters are obtained based on both input and output measurements [8]. Due to improvements in computing capacity, technological advances and developments in sensors and data acquisition systems, these analysis techniques can also be applied in SHM systems for civil infrastructures. In SHM, modal analysis is often applied as a form of Operational Modal Analysis (OMA) [14]. The major difference between OMA and EMA is that the input forces of OMA are unknown, and only the output measurements are available. Considering a highway bridge under normal

in-service conditions, the input forces may include various vehicles and environmental effects, such as wind and temperature changes, influences which are difficult to measure or quantify. Unfortunately, various techniques upon which EMA relies are invalid for OMA.

Driven by the demand for assessing the health of civil structures, a number of powerful techniques for OMA have been developed. Some common techniques are the Peak-Picking (PP) method [113, 114], the Auto Regressive-Moving Average Vector model [115], the Natural Excitation Technique (Next) [5, 116], the Random Decrement Technique [117], the Frequency Domain Decomposition [6] and the Stochastic Subspace Identification (SSI) [11, 114, 118]. The SSI algorithm is known as one of the most robust methods for OMA measurements, and has already been successfully applied to infrastructures under operational conditions, such as bridges [50, 119], towers [114, 120], and buildings [121, 122]. In this chapter, we will employ both the PP and the SSI methods for modal analysis.

In reality, modal parameters are not only sensitive to structural damage and degradation, but also to varying operational and environmental loadings, such as traffic, humidity, wind and most importantly, temperature [43, 49]. The modal changes caused by these factors can be much larger than those caused by real structural damage or degradation [112]. For reliable modal analysis, we must distinguish the abnormal changes caused by operational or environmental inputs from normal changes due to damage and degradation [45, 50]. In this chapter, we will take the influence of temperature and vehicle mass into account.

In this chapter, we begin with introducing the procedure of data selection in Section 7.2, then apply two modal analysis methods: the PP method and the SSI method, to extract modal parameters from the selected dataset in Section 7.3, and finally analyse the influence of temperature and vehicle mass on modal parameters in Section 7.4.

7.2 Data Selection

The accuracy of modal analysis relies on the quality of the utilised datasets. To extract modal parameters correctly, we first need to select some datasets of high-quality. In this section, we illustrate the data selection task with a three-step procedure: sensor selection, traffic event detection and free vibration periods extraction.

7.2.1 Sensor Selection

In the sensor network, both strain and vibration signals respond to traffic events. The left two pictures in Fig. 7.1 illustrate one truck event in the time domain, for either sensor type. From these pictures, it is easy to see that the truck event in the strain signal is represented as a peak, which occurs when the vehicle is actually on the measured span, and disappears rapidly when the vehicle passes. The truck event in the vibration signal produces oscillations, which will last for a long period after the truck has passed, if it is not disturbed by subsequent vehicles. Based on this observation, it is reasonable to select the strain signal to recognise traffic events [54, 55]. To monitor and evaluate the health of the bridge, spectral analysis is one of the widely used methods [3]. The right two pictures of Fig. 7.1 (right) illustrate the spectrum of both the strain and vibration signal, which are produced by a Discrete Fourier Transform (DFT). It is clear that the spectrum of the vibration signal is more informative than that of the strain signal. So both the strain and vibration signals are employed in our experiments: first, we use the strain signal to detect traffic events, then conduct spectral analysis on the corresponding vibration signal.

Since there are 91 strain sensors and 34 vibration sensors in our sensor network, which sensors are suitable? One simple standard of choosing strain sensors is that they can clearly represent traffic events. That is to say, the peak of the selected strain signal should have a strong amplitude. We choose one truck event on each side of the bridge as excitation, look into the response of all of the strain sensors, and finally choose one sensor on each side of the bridge as target. The selection

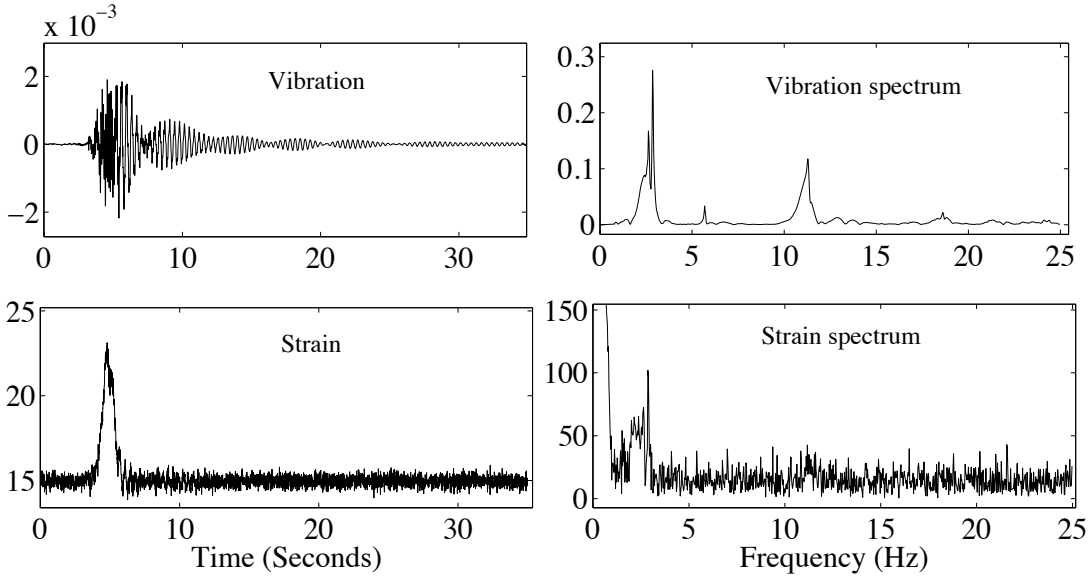

Figure 7.1: The strain and vibration signal in the time and frequency domain - The top left picture is a vibration signal; the top right picture is the spectrum of the vibration signal; the bottom left picture is a strain signal; the bottom right picture is the spectrum of the strain signal.

of the vibration sensors is based on the strain and vibration correlation matrix as mentioned in Chapter 4. We choose the vibration sensors that have strong correlations with the selected strain sensors as the target vibration sensors.

7.2.2 Traffic Event Detection

Following the procedure mentioned above, we obtain a pair of strain and vibration sensors installed on each side of the bridge, reducing the sensor candidates from 125 $(91 + 34)$ to 4 $(2 + 2)$. However, extracting traffic events from the reduced sensor signals is still a challenging task, because the bridge is a complex system, which responds to various inputs. As mentioned in previous chapters, some inputs play disturbing roles. What's more, even a useful input, such as a car or a truck, on one side of the bridge could not be detected or mis-detected in the signal collected with sensors on another side of the bridge. To prepare some high-quality datasets for modal analysis, we propose a procedure to extract traffic events. We

prefer that each target dataset just contains a single truck event. The procedure is listed as follows:

- **Step 1**: Find baseline. The baseline of the strain signal is influenced a lot by temperature and traffic jams. To measure the amplitudes of peaks correctly, we must find the baseline first.
- **Step 2**: Remove baseline. Baseline removal is quite straightforward. It is obtained by subtracting the baseline from the original strain signal.
- **Step 3**: Find peaks. Using the zero-crossing and the local maximum methods, we detect a number of peaks, with amplitude, duration and area under the peak as peak descriptive features.
- **Step 4**: Label peaks. Based on the video stream, we hand-label each peak as either of noise, car on lane 1, truck on lane 1, car on lane 4 or truck on lane 4. This will be our supervised training data (lane 1 and lane 4 stand for two different traffic directions).
- **Step 5**: Classify peaks. Based on the obtained peak features and labels, we try to find the boundaries between each class, by means of classification techniques from the Data Mining field [123].
- **Step 6**: Extract truck events. One whole traffic event is composed of the traffic-free period before the traffic peak, the actual peak and the traffic-free period after the traffic peak. We should look into the traffic events on both lanes to catch all traffic.

We choose a dataset of one hour at 3:00 AM (100 Hz) as the training dataset. The traffic during this time is not too heavy, and most of time there is just a single lane on either side in use. The baseline correction method mentioned in Step 1 and Step 2 is the most-crossing method, which was proposed in Chapter 5. After removing baselines from the selected strain signals, we continue to process the obtained signals with zero-crossing and local maximum methods in Step 3, achieving a number of peaks, with amplitude, duration and area under the peak as peak features. In Step 4, we hand-label these detected peaks according to the video taken during this period on the bridge. All the peaks are given one of five

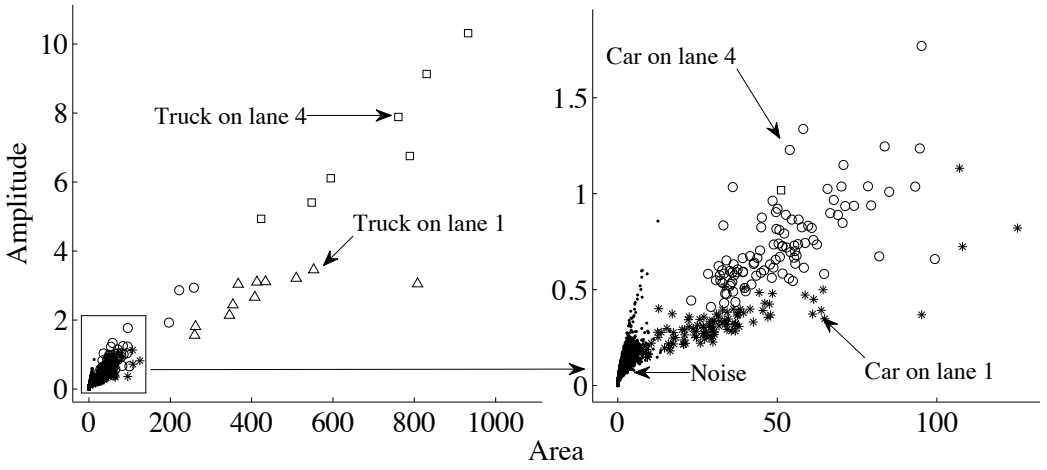

Figure 7.2: Peak classification - All peak labels within one hour (left), based on two peak features: area and amplitude; the right picture shows the details in the bottom left corner of the left picture, shown as the rectangular box in the left picture.

categories: noise, car on lane 1, truck on lane 1, car on lane 4 and truck on lane 4. The scatter plot based on area and amplitude of the strain peaks on lane 4 is illustrated as Fig. 7.2.

From the labels in Fig. 7.2, we can see that truck events on either lane are easy to distinguish, but the boundaries between car events on opposite lanes and the boundaries between the noise and car events on opposite lanes are blurry. When cars on an opposite lane are not heavy enough, they are easily mistaken as noise in the strain signal of the current lane. But the vibration sensor is much more sensitive to traffic events than the strain sensor, which can catch a small car event on another lane. To detect the complete free vibration period according to the strain signal, we must make the boundaries as clear as possible.

We processed our labeled peaks with Weka [123], a powerful Data Mining tool. A decision tree (C4.5) was applied to the labeled dataset (peak features), which takes *area* and *amplitude* on lane 4 as attributes.

The labeled dataset (derived from the training dataset) is composed of 7,169 instances, of which 7,137 (99.55%) instances are correctly classified. The confusion

Table 7.1: The confusion matrix.

truck 4	truck 1	car 4	car 1	noise	
7	0	1	0	0	truck 4
1	10	0	0	0	truck 1
0	2	97	4	0	car 4
0	0	3	98	4	car 1
0	0	2	15	6,925	noise

matrix is shown as Table 7.1.

The result, with a few minor mistakes, is already quite good, but can be further improved by combining the traffic events on the lane of opposite traffic direction (lane 1). We applied this model to a bigger dataset (the test dataset), which was obtained by selecting one hour per day at 3:00 AM for 45 days. We succeeded to catch 17,220 traffic events (of which 852 are trucks) on lane 1 and 13,064 traffic events on lane 4 (of which 768 are trucks). Truck events are usually featured with high amplitudes and peak areas, which indicate that the bridge is well excited, so we prefer to utilise the datasets caused by them for modal analysis. However, not every truck event is interesting to us. We expect that the vibrations caused by one truck should be long enough for modal analysis, without being disturbed by other traffic events. To meet this expectation, we explore truck events with long free vibration periods.

7.2.3 Free Vibration Periods Extraction

In this section, we focus on extracting the free vibration periods of traffic events from our structural health monitoring system, which is a critical step to analyse the modal parameters of the bridge. The free vibration period means the period after a vehicle has passed, and before a next vehicle appears on the bridge. The reason for choosing this period is that the bridge is put in motion by the vehicle, but the actual weight does not actually influence the frequency of vibration after the vehicle has disappeared, nor do any other vehicles.

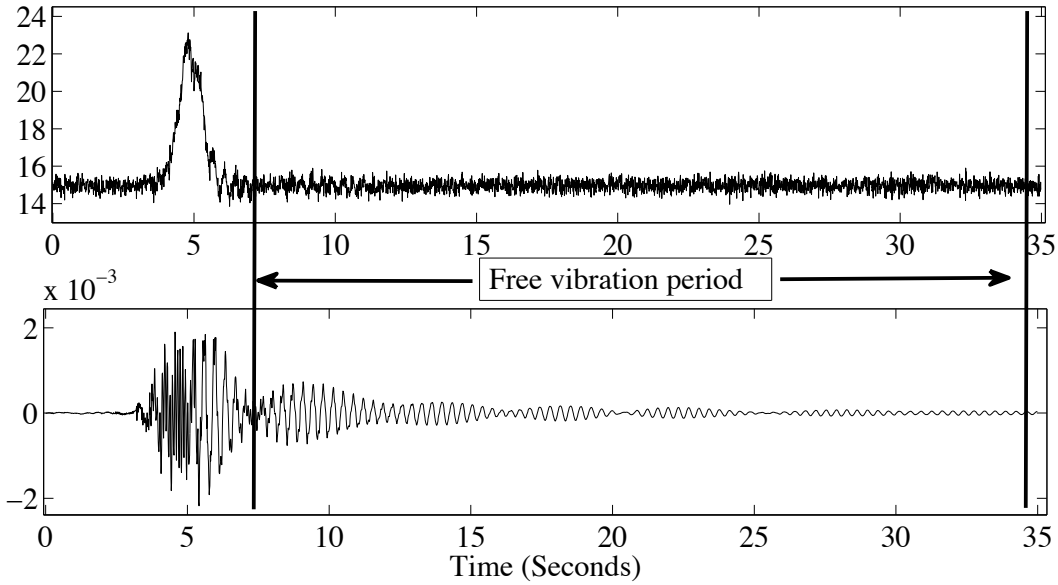

Figure 7.3: Free vibration period - The period between two vertical lines is referred to as the free vibration period, which starts after one truck just passes the bridge and ends before another vehicle appears on the bridge.

Shown as Fig. 7.3, free vibration fragments are extracted from the vibration signal, which corresponds to the traffic-free period directly after a truck-related peak in the strain signal. Details of how such periods can be identified in the data can be found in [53]. Following this procedure, we obtain a number of free vibration periods, which will be used for modal analysis in the next section.

7.3 Modal Parameter Extraction

In this section, we employ two methods to extract modal parameters: the PP method and the SSI method. The dataset employed for modal analysis is obtained by extracting truck events, with at least 20 seconds of free vibration period, from the testing dataset in the previous section, which is composed of 72 truck events on lane 1 and 77 truck events on lane 4.

7.3.1 The Peak-Picking Method

The PP method is a widely-used method to estimate modal parameters from output-only measurements [124, 125], in which the natural frequencies are simply obtained by choosing the peaks on the graphs of the power spectral densities (PSDs) [126, 127, 128]. The PSDs are basically obtained by converting the measurements to the frequency domain with the DFT [114, 127].

To obtain all the possible modes of the bridge, we apply the PP method to the free vibration periods of the selected dataset. After normalising the 149 spectra, we obtain a graph, shown as Fig. 7.4. From this figure, we can easily detect several interesting modes. Table 7.2 provides statistics of these modes. The approximate location of each mode is defined according to Fig. 7.4, and the occurrence of a mode is counted if there is at least one peak, whose amplitude is bigger than the average amplitude. The third column in Table 7.2 is calculated by counting what fraction of the 149 spectra actually show a peak at the specified location in the spectrum.

Table 7.2: Statistics of modes.

Mode	Frequency (Hz)	Occurrence
1	0.73 – 0.93	71.8%
2	2.59 – 2.78	100%
3	2.79 – 2.98	100%
4	5.50 – 5.77	97.3%
5	11.00 – 11.50	98.7%
6	14.82 – 15.55	12.1%
7	16.30 – 16.90	10.7%
8	18.30 – 18.80	48.3%

As illustrated below, the amplitude indicates the strength of each mode. Mode 2 and mode 3 are the principal modes of the bridge, which occur in every event. Mode 4 and mode 5 are also important modes, which have a strong amplitude and happen in most events. Mode 1 and mode 8 have moderate occurrence, but

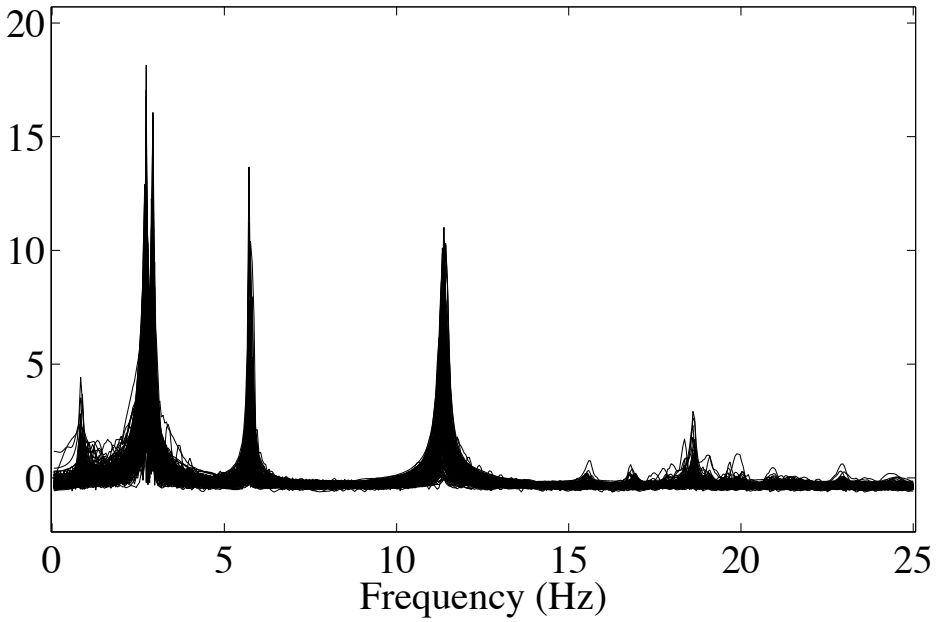

Figure 7.4: The vibration modes of the bridge - The spectra are derived from free vibration periods of 149 selected truck events.

their amplitudes are relatively weak. Mode 6 and mode 7 are so weak that they can be ignored in most cases.

The PP method is simple, and needs no model to fit to the measurements [113], so its identification is fast [128], and can be used on-site to verify the quality of the measurements [8, 114]. However, the PP method relies heavily on the frequency resolution [129]. When the assumptions of well separated modes and low damping are violated, the PP method often results in inaccurate and erroneous modes [8, 127]. To estimate modal parameters more accurately, we need employ more advanced methods.

7.3.2 The SSI Method

Compared with the PP method, the SSI method is a more advanced method for modal analysis. which is based on the stochastic state space model. To improve the result of the SSI method, the stabilization diagram is introduced to

distinguish physical modes from spurious modes. In this section, we will illustrate this method with some selected datasets, and present modal parameters derived from these datasets.

7.3.2.1 Stochastic State Space Model

The SSI method is especially suited for operational modal parameter identification when only output measurements are available. In the text below, the core steps of the SSI method are discussed. A detailed explanation is beyond the scope of this chapter and can be found in the references [11, 118]. The dynamic system of a vibration structure can be modelled by the following discrete-time state space model:

$$\begin{aligned} x_{k+1} &= Ax_k + Bu_k + w_k \\ y_k &= Cx_k + Du_k + v_k \end{aligned} \tag{7.1}$$

where y_k is the measurement at discrete time instance k, x_k is the state vector, u_k is the input vector, A is the discrete state matrix, B is the discrete input (system control influence coefficient) matrix, C is a real output influence coefficient matrix and D is the out control influence coefficient matrix; w_k is the process noise due to disturbances and modelling inaccuracies, and v_k is the measurement noise due to sensor inaccuracy. Here, the process noise w_k and measurement noise v_k are assumed to be white noise vectors, with the following covariance matrices:

$$E\left[\begin{pmatrix} w_p \\ v_p \end{pmatrix} \begin{pmatrix} w_q^T & v_q^T \end{pmatrix}\right] = \begin{bmatrix} Q & S \\ S^T & R \end{bmatrix} \delta_{pq} \tag{7.2}$$

where $E[\cdots]$ is the mathematical expectation operator, δ_{pq} is the Kronecker delta, and Q, R, S are process and measurement noise auto/cross-covariance matrices. The sequences w_k and v_k are assumed statistically independent of each other. In practice, the input vector u_k is not measured, and only the response of a structure is measured, so it is impossible to distinguish u_k from the process noise w_k and the measurement noise v_k. By implicitly modelling u_k with the noise terms w_k, v_k, the discrete-time stochastic state space model can be represented as:

$$\begin{aligned} x_{k+1} &= Ax_k + w_k \\ y_k &= Cx_k + v_k \end{aligned} \tag{7.3}$$

Here the noise terms w_k, v_k still follow the white noise assumption. One drawback of the stochastic state space model is that if the input contains some dominant frequency components except for the white noise, these frequency components will appear as poles of the state matrix A.

Estimation of state matrices Based on Eq. 7.3, there are several techniques that can be used for system identification through ambient measurements. The technique employed in this chapter is called data-driven stochastic subspace identification. All the output measurements are organized in a block Hankel matrix $H \in R^{2li \times j}$ with $2i$ block rows and j columns (each data point in the measurement is viewed as one column). Every block consists of l rows. For statistical reasons, it is assumed that $j \to \infty$. The block Hankel matrix H can be represented as:

$$H = \frac{1}{\sqrt{j}} \left[\begin{array}{cccc} y_0 & y_1 & \cdots & y_{j-1} \\ y_1 & y_2 & \cdots & y_j \\ \vdots & \vdots & \vdots & \vdots \\ y_{i-1} & y_i & \cdots & y_{i+j-2} \\ \hline y_i & y_{i+1} & \cdots & y_{i+j-1} \\ y_{i+1} & y_{i+2} & \cdots & y_{i+j} \\ \vdots & \vdots & \vdots & \vdots \\ y_{2i-1} & y_{2i} & \cdots & y_{2i+j-2} \end{array}\right] = \left[\frac{Y_{0|i-1}}{Y_{i|2i-1}}\right] = \left[\frac{Y_p}{Y_f}\right] \tag{7.4}$$

where $\frac{1}{\sqrt{j}}$ is the scaled factor, Y_p stands for the past output matrix, Y_f represents the future output matrix. The key element of the data-driven SSI is the projection of the row space of the future outputs into the row space of the past outputs. This projection can be defined as:

$$P_i = \frac{Y_f}{Y_p} = Y_f Y_p^T (Y_p Y_p^T)^\dagger Y_p \tag{7.5}$$

where $(\cdot)^\dagger$ represents the pseudo-inverse of a matrix.
The projection P_i can be factorised as:

$$P_i = \Gamma_i X_0 = \begin{bmatrix} C \\ CA \\ CA^2 \\ \dots \\ CA^{i-1} \end{bmatrix} \begin{bmatrix} x_0 & x_1 & x_2 & \dots & x_{i-1} \end{bmatrix} \tag{7.6}$$

where Γ_i is the observability matrix, and X_0 represents the Kalman filter state sequence at time lag zero. With the help of the singular value decomposition (SVD), the projection P_i can be further decomposed as:

$$Y_i = USV^T = \begin{bmatrix} U_1 & U_2 \end{bmatrix} \begin{bmatrix} S_1 & 0 \\ 0 & S_2 \end{bmatrix} \begin{bmatrix} V_1^T \\ V_2^T \end{bmatrix} = U_1 S_1 V_1^T \tag{7.7}$$

The order n of the system can be determined by neglecting the smaller singular values in S_2, and the observability matrix Γ_i and Kalman filter state sequence X_0 can be estimated by:

$$\begin{aligned} \hat{\Gamma}_i &= U_1 S_1^{1/2} \\ \hat{X}_0 &= S_1^{1/2} V_1^T \end{aligned} \tag{7.8}$$

The system parameter matrices A and C can be obtained based on the estimated observability matrix $\hat{\Gamma}_i$:

$$\begin{aligned} A &= \hat{\Gamma}_{i1}^{\dagger} \hat{\Gamma}_{i2} \\ C &= \hat{\Gamma}_{li} \end{aligned} \tag{7.9}$$

where $\hat{\Gamma}_{i1}$ denotes $\hat{\Gamma}_i$ without the last l rows, $\hat{\Gamma}_{i2}$ represents $\hat{\Gamma}_i$ without the first l rows, and $\hat{\Gamma}_{li}$ stands for the first l rows of $\hat{\Gamma}_i$.

Modal parameters The modal parameters are derived from the system parameter matrices A and C:

$$\begin{aligned} A &= \Psi \left[\mu_i\right] \Psi^{-1} \\ f_i &= \frac{|\lambda_i|}{2\pi} \\ \xi_i &= \frac{Re(\lambda_i)}{|\lambda_i|} \\ \Phi &= C\Psi \end{aligned} \tag{7.10}$$

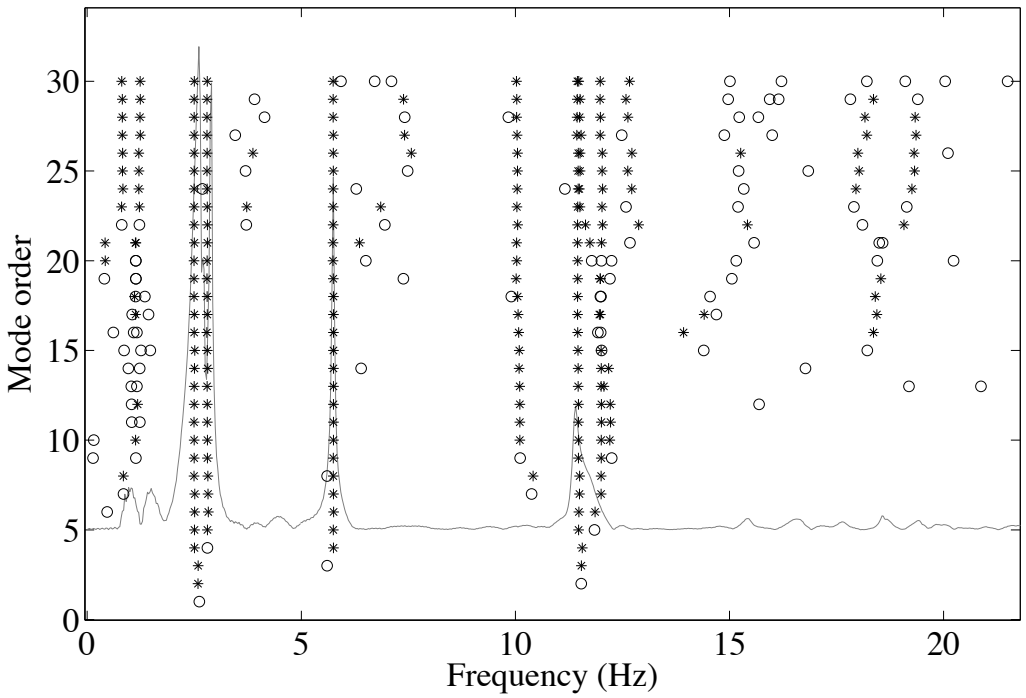

Figure 7.5: The stabilization diagram - The stabilization diagram is obtained by setting the stable criteria as 5% for natural frequencies and MAC, in which the stars represent stable physical poles, and the circles represent the spurious poles; the background spectrum is derived from the PP method.

where Ψ is the matrix of eigenvectors, μ_i are the discrete time poles, $\lambda_i = \frac{\ln(\mu_i)}{\Delta T}$ are the continuous poles, f_i are the natural frequencies, ξ_i are the damping ratios, and Φ is the mode shape matrix.

7.3.2.2 The Stabilization Diagram

It is assumed that all the input forces of the SSI procedure are white noise and the length of the recording is infinite. In practice, the measurements used for SSI are limited, and usually contain some other dominant frequency components. As shown in Eq. 7.5, the order of the system is obtained by ignoring the smaller singular values, which is usually higher than the actual system order. All of these factors may introduce spurious, numerical poles to the system. To address

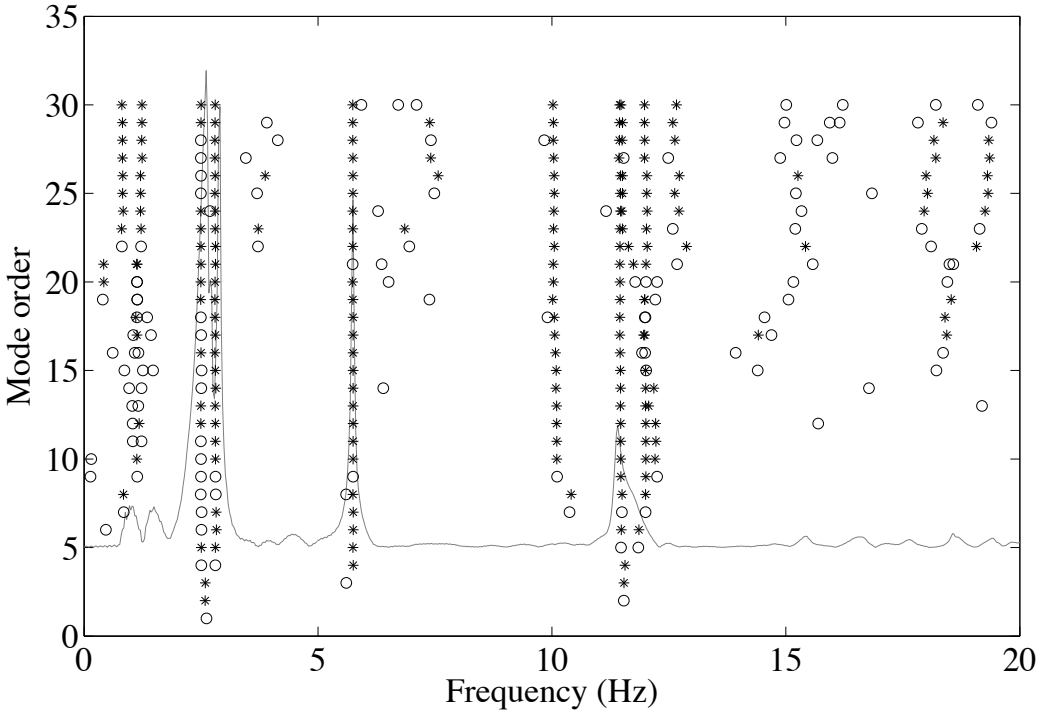

Figure 7.6: The stabilization diagram - The stabilization diagram is obtained by setting the stable criteria as 5% for natural frequencies and MAC, and 50% for damping ratios, in which the stars represent stable physical poles, and the circles represent the spurious poles; the background spectrum is derived from the PP method.

the physical and the spurious, numerical poles, the stability diagram [130] is introduced. The basic idea of the stabilization diagram is to iterate the system order n from a lower value to the maximum order. It is assumed that the lowest order is unstable, so the modal parameters of the current order are compared with those of one order lower. If the differences are under user-defined limits, then this order is considered to be a stable order. The limits are defined as:

$$\begin{aligned} \left| \frac{f_k - f_{k-1}}{f_k} \right| &< lim_f \\ \left| \frac{\xi_k - \xi_{k-1}}{\xi_k} \right| &< lim_\xi \\ (1 - MAC(k, k-1)) &< lim_{MAC} \end{aligned} \tag{7.11}$$

where $k > 1$ denotes the modal order, f is the frequency, ξ is the damping ratio, lim_f is the frequency limit, lim_ξ is the limit for the damping, lim_{MAC} is the limit for the modal assurance criterion (MAC). The MAC value ranges from 0 to 1, where 0 means that there is no similarity between the compared mode shapes, and 1 means these two mode shapes are consistent. The MAC can be defined as:

$$MAC(k, k-1) = \frac{|\Phi_k^H \Phi_{k-1}|^2}{(\Phi_k^H \Phi_k)(\Phi_{k-1}^H \Phi_{k-1})} \tag{7.12}$$

7.3.2.3 Experimental Settings on InfraWatch Dataset

To employ the SSI method for modal analysis, we select a dataset derived from 12 vibration sensors in the sensor network. The sensors are located at three cross-section of four different girders, which are equally spaced in both longitudinal and transversal directions.

The first activity to extract modal parameters from measurements with the SSI method, is creating a Hankel matrix with 24 block rows (30 rows per block), and 3,377 columns. One key parameter for SSI is the order of the system. Because of operational noise, it is impossible to obtain the system order precisely from the singular value of the Hankel matrix projection. If the system order is estimated with a lower value, some physical poles will be missed. Otherwise, spurious numerical poles may appear. The stabilization diagram is useful to separate physical poles from spurious numerical poles. In the stabilization diagram, the system order is tested from a minimal order 2 to a maximum order of 30. The physical poles are represented as stars and spurious poles are represented as circles. We assume the initial status of each pole is unstable, e.g, the two poles of mode order 2 are represented as circles.

The stable criteria are set as 5% for natural frequencies, and 5% for MAC. In practice, the damping ratios are difficult to be estimated accurately [131]. Shown in Fig. 7.5, the stabilization diagram is obtained by just employing natural frequencies and MAC stable criteria. The stabilization diagram in Fig. 7.6 is obtained

Table 7.3: Modal Parameters.

Mode	Mode shape	Frequency (SSI)	Frequency (PP)	Relative error
1	Bending	2.51 Hz	2.61 Hz	4.0%
2	Torsional	2.81 Hz	2.90 Hz	3.2%
3	Bending & Torsional	5.74 Hz	5.75 Hz	0.2%
4	Bending	10.09 Hz	–	–
5	Torsional	11.47 Hz	11.41 Hz	−0.5%
6	Bending & Torsional	11.99 Hz	–	–

by setting damping ratio criterion to a higher value (50%). Even when the stable criterion for damping ratios is much higher than that of natural frequencies and MAC, there is still one mode (around 2.51 Hz), that can be clearly observed from the background spectrum (derived from the PP method to one of the selected 12 vibration signals), is mistaken as a spurious mode. In this experiment, we exclude the damping ratio criterion from the stable criteria.

7.3.2.4 The Results of the SSI Method

The results of SSI method includes: natural frequencies, mode shapes and damping shapes. As illustrated in the stabilization diagram Fig. 7.6, damping ratios obtained with the SSI method are unreliable, so we won't further discuss them in this chapter. The results of the first two parameters are listed as follows:

Natural frequency We make a comparison between the modes obtained with the SSI method and the PP method, shown as Table 7.3. From both the table and the stabilization diagrams, we notice that there is a high coherence between the peaks in the spectrum and physical poles obtained with the SSI method. However, with the SSI method, we can obtain more poles, e.g, the modes around 10 Hz and 12 Hz, which are absent in the PP method, and there are some small peaks in the spectrum that are identified as spurious modes, e.g, the modes between 0.7 Hz and 1 Hz.

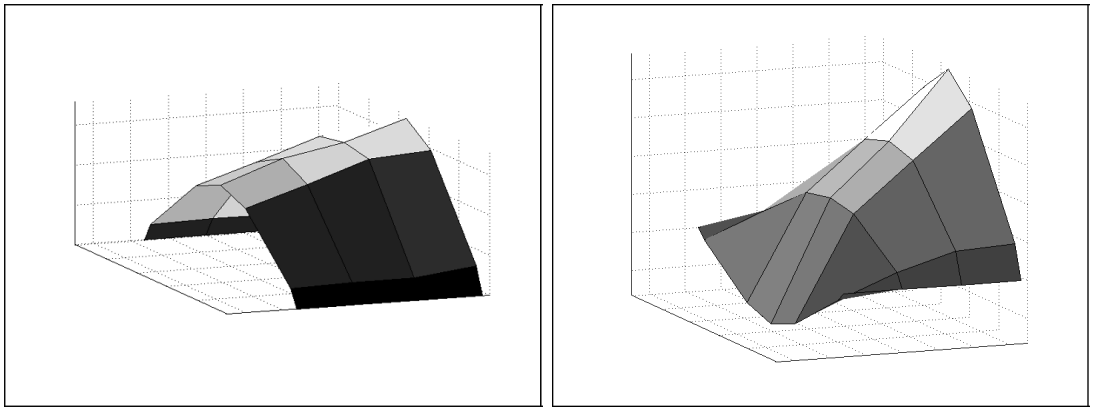

Figure 7.7: The first and the second mode shapes - The left picture shows the mode shape of the first mode, which is the first bending mode. The right picture shows the mode shape of the second mode, which is the first torsional mode.

Compared with the modes in Table 7.2, Table 7.3 has fewer modes. This is because not all the modes of a bridge can be excited by a single traffic event at the same time. The modes in the former table are derived from 149 truck events, and the results in the latter table are derived from a single truck event.

Mode Shapes Fig. 7.7 to Fig. 7.9 show the first six mode shapes derived from the SSI method. Because the sensor network just covers half of the bridge span, the mode shapes of the unmeasured half span are modelled using the existing measurements and structural knowledge.

7.4 The Influence of Environmental Factors

As mentioned in Section 7.1, modal parameters are not only sensitive to structural damage and degradation, but also to varying operational and environmental loadings, which include traffic, wind, humidity and temperature. In this section, we will look into the influence of temperature and vehicle mass on one of the most important modal parameters: natural frequencies.

If we simply take the bridge as a Euler-Bernoulli beam, the vehicle and bridge

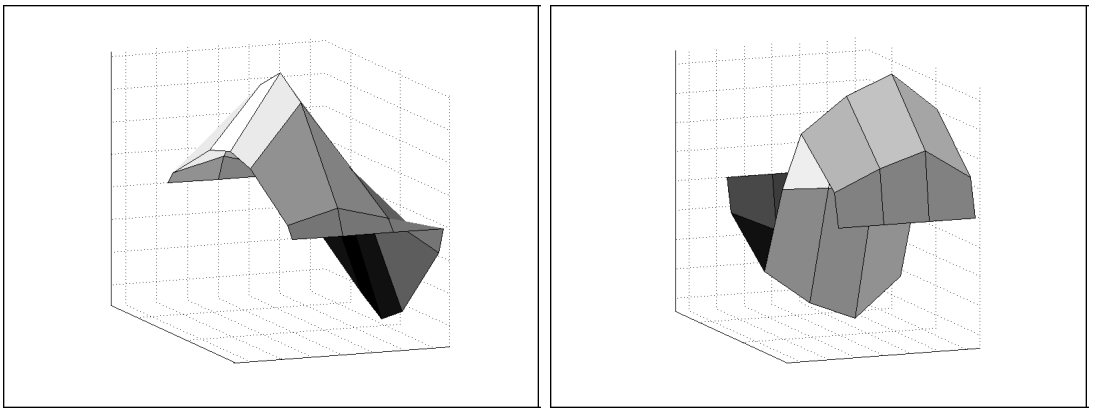

Figure 7.8: The third and the fourth mode shapes - The left picture shows the mode shape of the third mode, which is the first mixed mode, derived from the combination of bending and torsional behaviour. The right picture shows the mode shape of the fourth mode, which is the second bending mode.

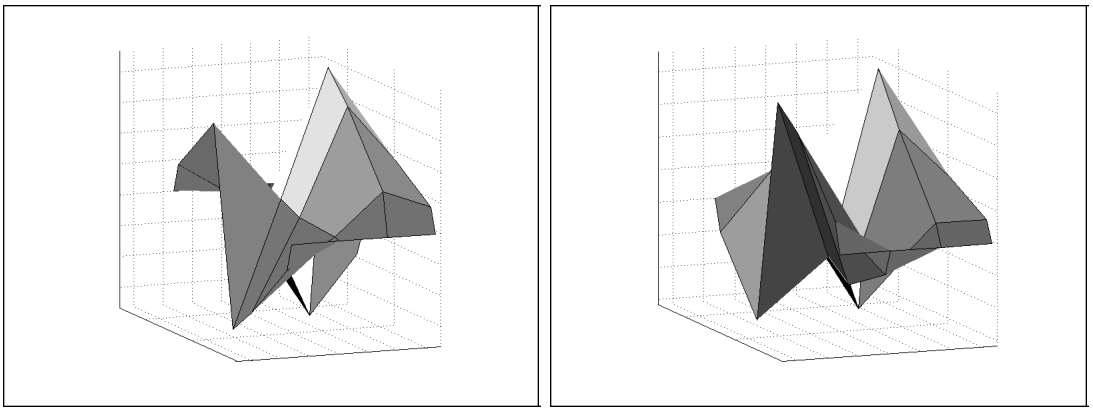

Figure 7.9: The fifth and the sixth mode shapes - The left picture shows the mode shape of the fifth mode, which is the second torsional mode. The right picture shows the mode shape of the sixth mode, which is the second mixed mode, composed of bending and torsional behaviour.

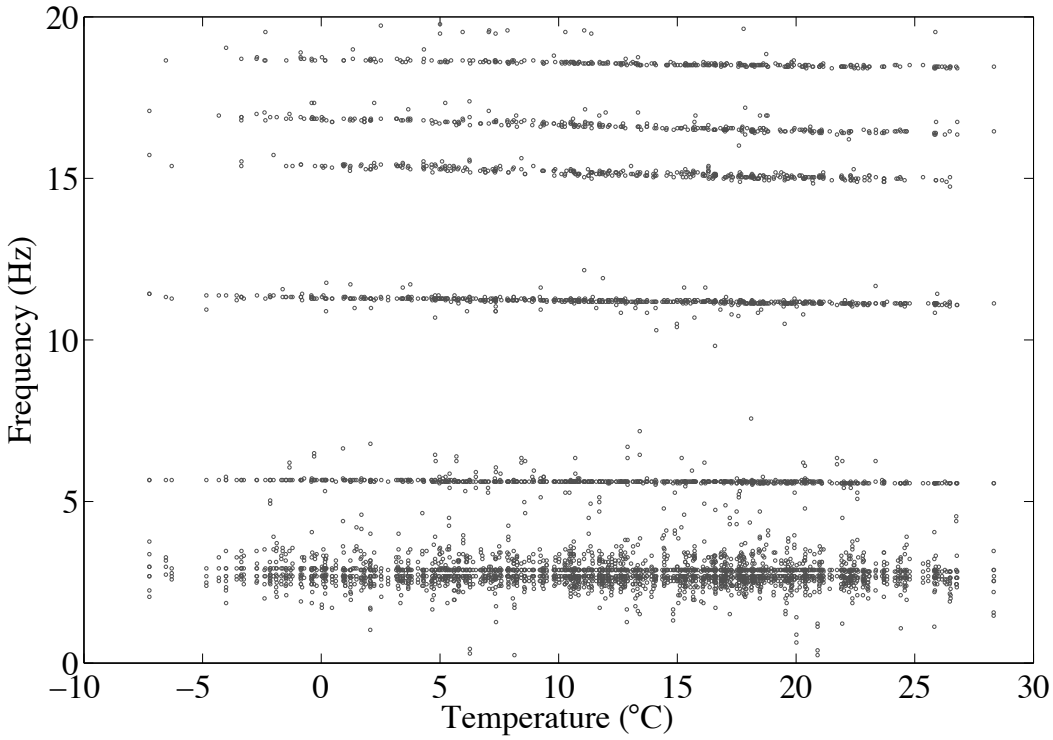

Figure 7.10: Natural frequencies and temperature - This picture illustrates a scatter plot between natural frequencies and temperature, in which natural frequencies derived from free vibration periods of 983 truck events; the data covers a period of more than two years, with a temperature range of 40 °C.

interaction system [132] can be modelled as a damped parallel spring mass system, and each natural frequency f_n of the system can be represented as follows:

$$f_n = \frac{1}{2\pi}\sqrt{\frac{k}{m}} \tag{7.13}$$

where k represents for the stiffness of the bridge, m represents the total mass on the bridge. According to Peeter et al. [50], the temperature may have an impact on the boundary conditions and the Young's modulus of the material of which the structure consists. The variation of temperature will cause changes in the stiffness k of the bridge, and vehicles on the bridge will add to the mass m. All these changes can be detected from the measurements collected from the bridge.

The dataset employed in this section covers a big time scale, ranging from January, 2009 to September, 2011. We select 5 minutes (100 Hz) at 1:00 AM from each day, and extract truck events with long free vibration periods. Following the procedure mentioned in Section 7.2, we obtain 983 truck events with free vibration periods longer than 1,024 data points (10.24 seconds). The method employed for modal analysis is the PP method, because of its simplicity and high coherence with the advanced SSI method.

7.4.1 The Influence of Temperature

To look into the influence of temperature on natural frequencies, we employ the free vibration periods of the selected 983 truck events. During the free vibration period, the bridge has already been excited by the vehicle, but the weight of the truck no longer influences the total bridge mass, so it helps to separate the influence of temperature from the influences of other factors.

We choose a free vibration period of 2,048 data points (slightly over 20 seconds long) from each truck event collected with a vibration sensor, and apply the PP method for modal analysis. The temperature of the bridge is estimated by the average value of one of the temperature sensors during the free vibration period. Shown as Fig. 7.10, the temperature of our selected truck events ranges from -8 °C to 32 °C, and there are clearly several modes within the first 20 Hz. By zooming in the scatter plot, we find out that the mode between 2 and 5 Hz is actually composed of two modes, so there are 7 modes visible in the scatter plot. Generally speaking, the natural frequencies decrease with increasing temperature, but the influence of temperature on different modes is not equal. To look into the influence of temperature in detail, we fit each mode separately with a linear regression model, shown as Fig. 7.12 to Fig. 7.18[1]. The linear model can be represented as:

$$f = a \cdot t + b \tag{7.14}$$

[1]Note that the detailed plots of the modes show a discrete behavior along the Y-axis. This is caused by the resolution of the spectrum resulting from the FFT operation. With an input consisting of 2,048 measurements, the distance between frequency bins is 0.0488 Hz.

Table 7.4: The coefficients of linear regression models between temperature and natural frequencies.

Mode	a	b	norm	r
1	$-5.551 \cdot 10^{-4}$	2.678	$9.188 \cdot 10^{-4}$	0.188
2	$-1.731 \cdot 10^{-3}$	2.901	$8.550 \cdot 10^{-4}$	0.501
3	$-2.852 \cdot 10^{-3}$	5.651	$8.069 \cdot 10^{-4}$	0.736
4	$-7.587 \cdot 10^{-3}$	11.305	$1.420 \cdot 10^{-3}$	0.859
5	$-1.741 \cdot 10^{-2}$	15.387	$3.692 \cdot 10^{-3}$	0.868
6	$-1.732 \cdot 10^{-2}$	16.838	$3.722 \cdot 10^{-3}$	0.907
7	$-9.277 \cdot 10^{-3}$	18.676	$2.201 \cdot 10^{-3}$	0.868

in which a and b are coefficients, t stands for input (temperature), and f stands for the predicted frequency. The goodness of fit is measured by the *norm of residuals* as well as the *correlation coefficient* r. We give the definition of *norm of residuals*, which is:

$$norm(d, 2) = \frac{\sqrt{\sum_{i=1}^{n} d_i^2}}{n} \tag{7.15}$$

in which d_i stands for the difference between the i^{th} predicted value and the i^{th} actual value. The coefficients of each linear regression model are listed in Table 7.4, and a scatter plot between coefficients a and b is illustrated in Fig. 7.11.

From these linear regression models, we can draw the following conclusions:

- All the natural frequencies decrease with increasing temperature.
- Different modes have different sensitivity to temperature.
- High-frequency modes are more sensitive to temperature than low-frequency mode, except for the last two modes.

7.4.2 The Influence of Traffic Events

For short periods, the stiffness of the bridge can be assumed constant, and the only factor influencing the natural frequencies is the mass of traffic. We assume that when a truck is on the bridge, the mass of the bridge increases, and the

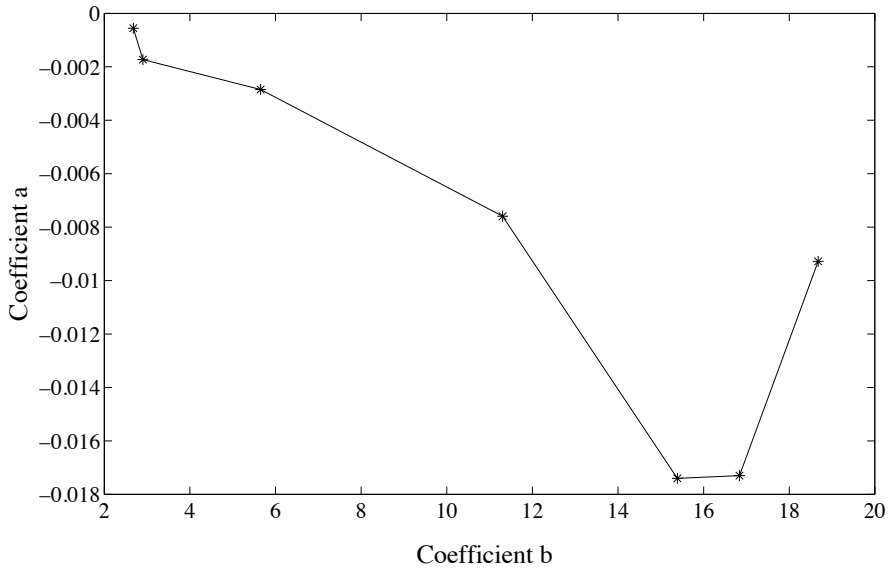

Figure 7.11: Coefficients of linear models - The Y-axis stands for the first coefficient (a) of the linear model; the X-axis stands for the second coefficient (b) of the linear model

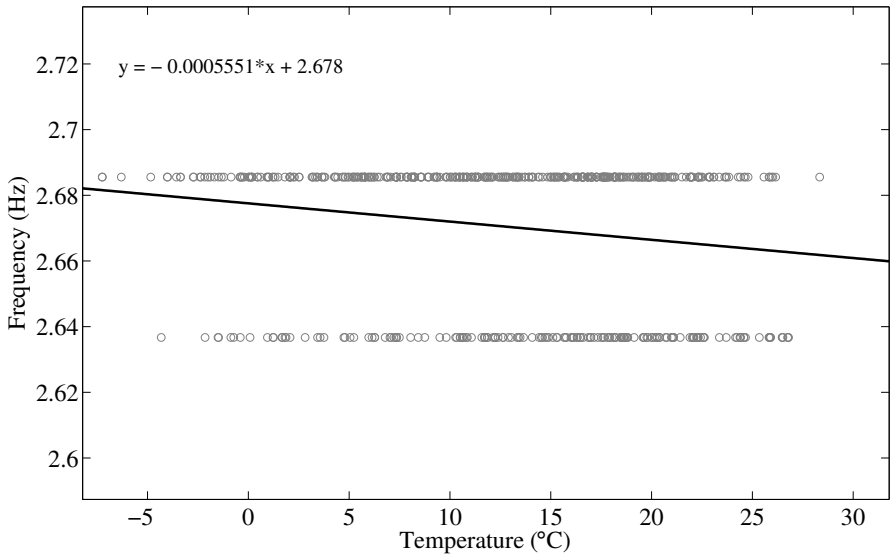

Figure 7.12: The linear modal between the first mode and temperature - The coefficients indicate that the first mode is practically insensitive to temperature.

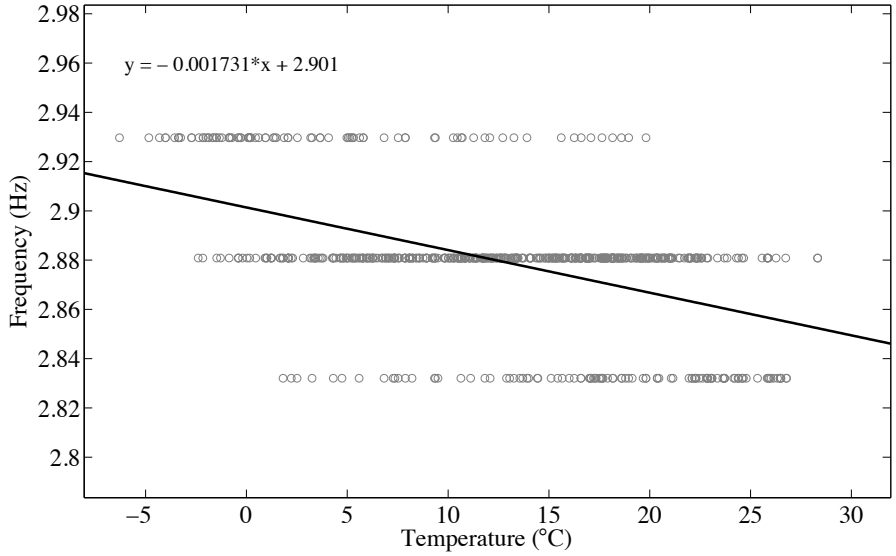

Figure 7.13: The linear modal between the second mode and temperature - The coefficients indicate that the second mode is more sensitive to the temperature than the first mode.

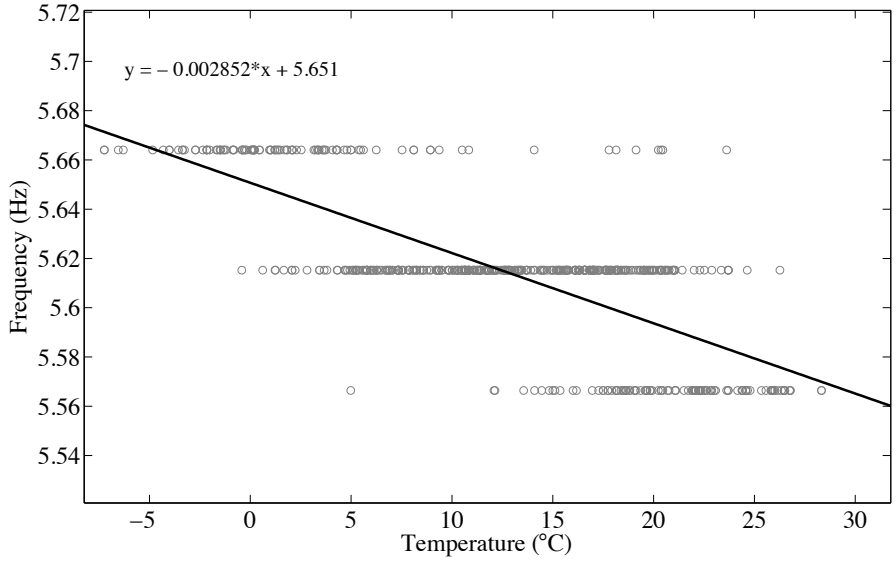

Figure 7.14: The linear modal between the third mode and temperature - The coefficients indicate that the third mode is more sensitive to the temperature than the first two modes.

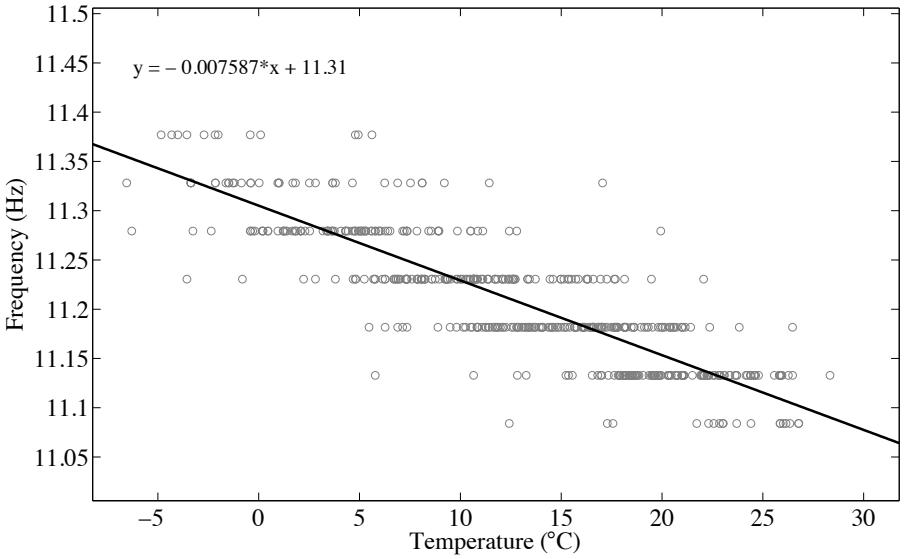

Figure 7.15: The linear modal between the fourth mode and temperature - The coefficients indicate that the fourth mode is more sensitive to the temperature than the first three modes.

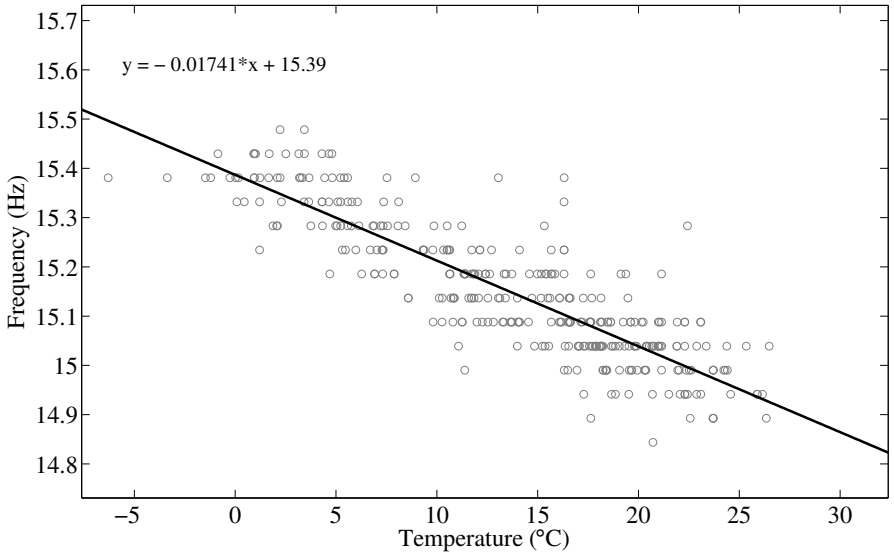

Figure 7.16: The linear modal between the fifth mode and temperature - The coefficients indicate that the fifth mode is more sensitive to the temperature than the first four modes.

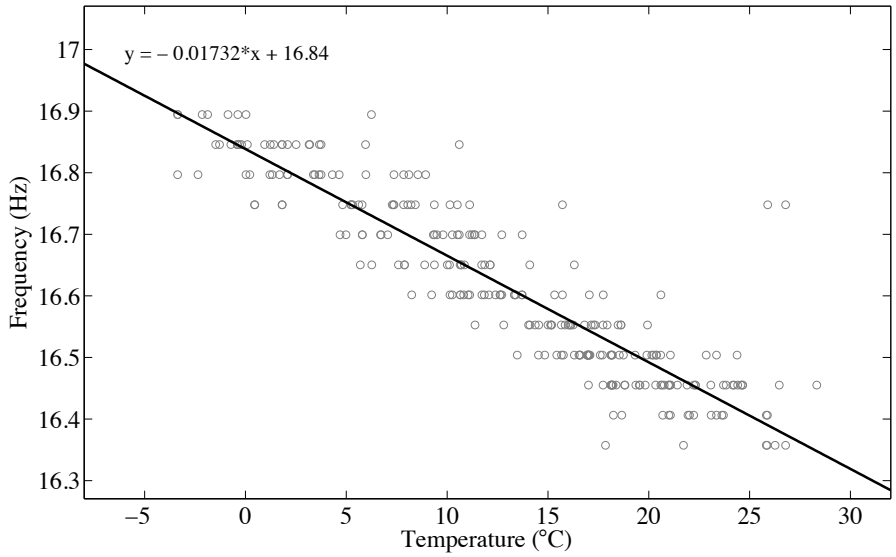

Figure 7.17: The linear modal between the sixth mode and temperature - The coefficients indicate that the sixth mode is less sensitive to the temperature than the fifth mode, but more sensitive than the first four modes.

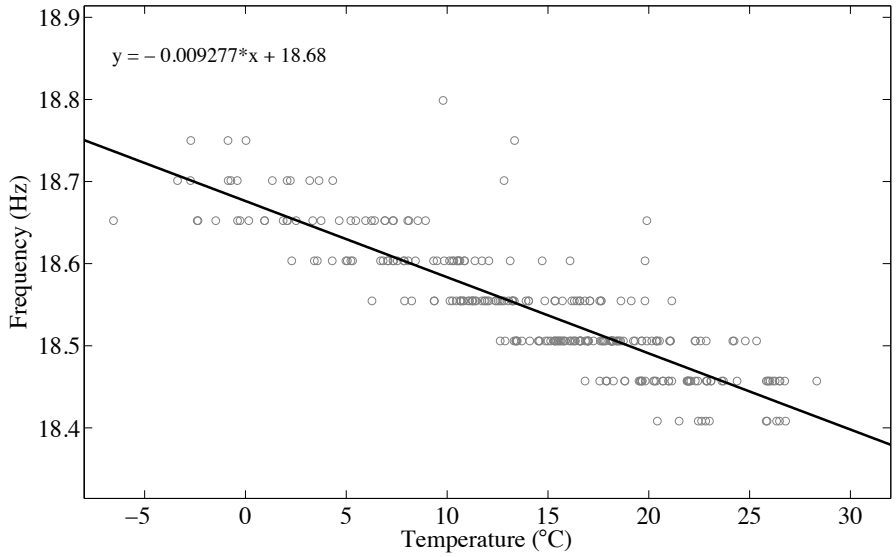

Figure 7.18: The linear modal between the seventh mode and temperature - The coefficients indicate that the seventh mode is more sensitive to the temperature than the first four modes, but less sensitive to the fifth and sixth modes.

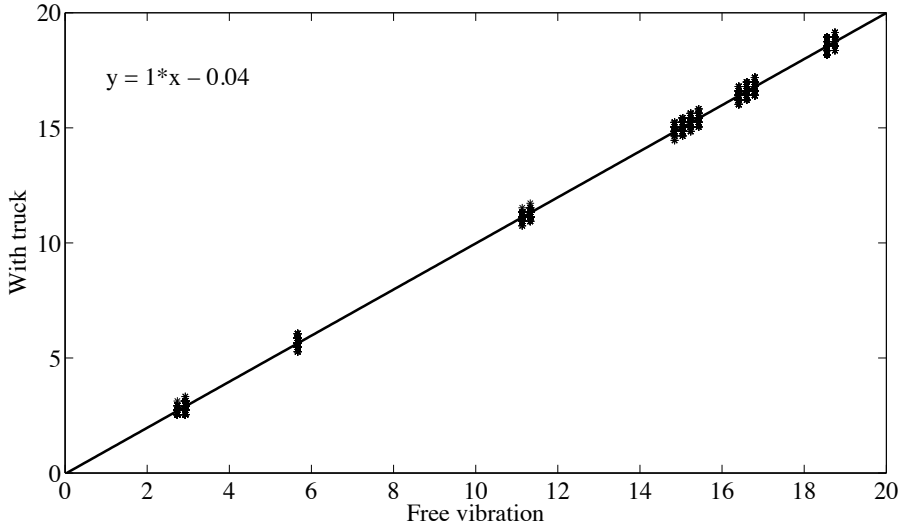

Figure 7.19: The influence of mass on all modes - This picture illustrates a scatter plot of natural frequencies obtained with trucks on the bridge and during free vibration periods.

natural frequencies should decrease. To verify the assumption, we apply DFT to the periods when trucks are on the bridge and the periods of free vibration respectively. As illustrated in Fig. 7.19, generally speaking, natural frequencies obtained with vehicles on the bridge are less than those obtained from free vibration periods. To look into the influence of traffic mass on each mode, we make a statistical analysis, shown as Table 7.5. In this table, $f_{free=mass}$ indicates that the frequency obtained during free vibration period is equal to the frequency obtained with a vehicle on the bridge; $f_{free>mass}$ indicates that the former frequency is bigger than the latter frequency; $f_{free<mass}$ indicates that the former frequency is smaller than the latter frequency.

The statistical results in Table 7.5 meet well with the linear function illustrated in Fig. 7.19, while the table reveals more details:

- In all the modes, most frequencies obtained with vehicles on the bridge are equal to frequencies obtained with free vibration periods.
- The numbers in columns 3 and 4 indicate that the mass of vehicles influences

Table 7.5: The statistical analysis of the influence of mass on each mode.

Modes	$f_{free=mass}$	$f_{free>mass}$	$f_{free<mass}$
1	106	58	34
2	407	327	30
3	467	110	102
4	571	261	40
5	433	190	155
6	300	196	120
7	306	128	104

the frequencies of all the modes, some of which are positive ($f_{free>mass}$), and some of which are negative ($f_{free<mass}$), and the positive numbers are bigger than the negative numbers.

- The positive numbers in mode 2 and 4 are bigger than the negative numbers, which indicates that these two modes are more sensitive to traffic mass. Referring to Table 7.3, we further find that both of these two modes are torsional modes.